Microchim Acta (2016) 183:863–869
DOI 10.1007/s00604-015-1734-y

ORIGINAL PAPER

Colorimetric determination of aluminum(III) based on the aggregation of Schiff base-functionalized gold nanoparticles

Pengcheng Huang[1] · **Jianfang Li**[1] · **Xin Liu**[1] · **Fangying Wu**[1]

Received: 8 October 2015 / Accepted: 13 December 2015 / Published online: 29 December 2015

Abstract The authors describe a colorimetric method for the determination of Al(III) using surface modified gold nanoparticles (AuNPs). Citrate capped AuNPs were functionalized, by self-assembly, with the Schiff base obtained from 2-hydroxy-1-naphthaldehyde and 2-aminoethanethiol. The modified AuNPs were characterized by transmission electron microscopy and FTIR. Complexation of Al(III) ions by the Schiff base on the AuNPs results in self-aggregation of the AuNPs which is accompanied by a color change from red to blue which can be monitored visually or by UV–vis spectroscopy. Absorbance varies linearly with the Al(III) concentration in the range from 9 to 23 μM, and the lower detection limit is 0.29 μM (at 3 S_o/k). The method was applied to the determination of Al(III) in (spiked) samples of boiler water and urine.

Keywords Spectrophotometry · Photometric assay · Visual detection · Transmission electron microscopy · FTIR · Self assembly

Introduction

Dissolved Al^{3+} widely exists in the environment due to acidic rain and human activities. Its toxicity not only hampers plant growth but also damages the human nervous system to induce Alzheimer's disease [1], Parkinson's disease [2], dialysis encephalopathy [3] etc. To avoid the adverse health problems caused by the uptake of Al^{3+}, an estimated tolerable dietary intake in the human body is 7 mg kg^{-1} body weight per week [4]. Detection of Al^{3+} is crucial in controlling its concentration levels in the biosphere and its direct impact on human health.

Al^{3+} is detected using multiple laboratory analysis platforms, including atomic absorption spectrometry [5], inductively coupled plasma mass spectroscopy (ICP-MS) [6], and voltammetry [7]. Although these methods can enable a high level of qualitative and quantitative analyses, operative inability by a non-specialist and requirement of sophisticated instrumentation severely limit applications which are suitable for point-of-care, field deployment, or other low-resource settings. To date, optical sensors, especially colorimetric ones, have always been the most convenient analytical tool and gained a lot of interest because they provide a simple and economical assay without the aid of instruments. It is reported that colorimetric chemosensors have been widely exploited for Al^{3+} detection [8–10], which depends on rational design of Al^{3+}-responsive receptors with sufficient or even remarkable sensitivity and selectivity. Although they provide a straightforward and acceptable assay, they always suffer from complicated probe design, multistep synthesis strategy and large reagent consumption. Besides, concerning their practical applications, aqueous media may be the best choice for Al^{3+} detection, but majority of these sensors are unstable or dysfunctional in aqueous solution.

Compared with chromophoric chemosensors, gold nanoparticles (AuNPs) based colorimetric assays have emerged as a fascinating research field [11–14]. AuNPs can be synthesized in a straightforward manner and remain highly stable after proper surface modification. They possess unique optical properties which depend on interparticle distance, i.e., dispersion/aggregation is directly

Electronic supplementary material The online version of this article (doi:10.1007/s00604-015-1734-y) contains supplementary material, which is available to authorized users.

✉ Fangying Wu
fywu@ncu.edu.cn

[1] College of Chemistry, Nanchang University, Nanchang 330031, China

observed as a solution color switch due to surface plasmon coupling. In addition, they have an high extinction coefficient (from 1×10^8 to 1×10^{10} M^{-1} cm^{-1}), which is often several orders of magnitude higher than those of organic dyes. More importantly, AuNPs have a high surface area to volume ratio, and their surfaces can be readily chemically tailored by ligands with functional groups. Through these functional groups, specific molecular recognition can be realized, thus allowing for easy colorimetric assays of a wide range of targets, including metal ions, small molecules, proteins, nucleic acids, malignant cells, etc., at fairly low concentrations. Although a large number of sensitive and reliable gold nanoparticle-based colorimetric detections of transition metal ions (Cd^{2+}, Pb^{2+}, Hg^{2+}, Cu^{2+}, etc.) have been introduced [15–21], colorimetric detection of Al^{3+} using AuNPs probe is not well studied. Li et al. reported the first colorimetric assay based on pentapeptide functionalized AuNPs for detecting Al^{3+}, which achieved great success at monitoring contaminated levels of Al^{3+} on living cellular surfaces [22]. Moreover, mononucleotide-modified metal nanoparticles were also reported as a colorimetric probe for selective and sensitive detection of Al^{3+} and used to monitor Al^{3+} on living cellular surfaces under physiological conditions [23].

To develop a convenient alternative for on-site Al^{3+} assay that meets the requirements of low cost, high sensitivity and selectivity, water compatibility and environment friendliness, we demonstrated a colorimetric assay for the detection of Al^{3+} based on the Al^{3+}-induced self-aggregation of AuNPs. The Schiff base of N-(2-hydroxynaphthylidene)-2-aminoethanethiol (HNAET) was synthesized and introduced as the chelating ligand on the surface of AuNPs through the well-known strong Au-S interaction (HNAET-AuNPs) (Scheme 1). The Schiff bases formed on the AuNPs surface may serve as efficient and selective complexing reagents for Al^{3+} rather than other metal cations [24]. In aqueous media, the affinity of Al^{3+} toward the functional naphthol group led to an interparticle crosslinking induced aggregation of HNAET–AuNPs and a clear color change from red to blue. Therefore, a colorimetric assay for visual detection of Al^{3+} was developed. Compared with the use of pentapeptide or mononucleotide modified AuNPs as the Al^{3+} probe [22, 23], this small molecular ligand-modified AuNPs probe is cheaper and readily achievable. More importantly, the HNAET–AuNPs probe matches the probes in terms of its analytical capacity.

Experimental

Instruments

Transmission electron microscope (TEM) measurements were performed on a JEM-2010 instrument (JEOL Ltd, Japan, www.jeol.cn). Absorption spectra were recorded on a Ultraviolet–visible (UV–Vis) 2550 spectrophotometer (Shimadzu, Kyoto, Japan, www.shimadzu.com) equipped with a 1 cm quartz cell. Nuclear magnetic resonance (NMR) data of the synthesized ligand were collected using a Agilent-400 MHz NMR instrument (Agilent Technologies Inc., USA, www.agilent.com). Fourier Transform Infrared Spectoscopy (FTIR) spectra were recorded on a Nicolet 5700 Fourier transform spectrometer (Nicolet, USA, www.thermonicolet.com). Mass spectra were obtained with a WatersZQ-4000 ion trap mass spectrometer (Waters Corporation, USA, www.waters.com). The zeta potentials and dynamic light scattering (DLS) of the samples were determined using a Zetasizer (Zetasizer nano zs90, Malvern Instruments, UK, www.malvern.com/en/).

Chemicals

Hydrogen tetrachloroaurate hydrate ($HAuCl_4 \cdot 4H_2O$) was obtained from Sinopharm Group (http://www.sinoreagent.com/). 2-hydroxy-1-naphthaldehyde and 2-aminoethanethiol

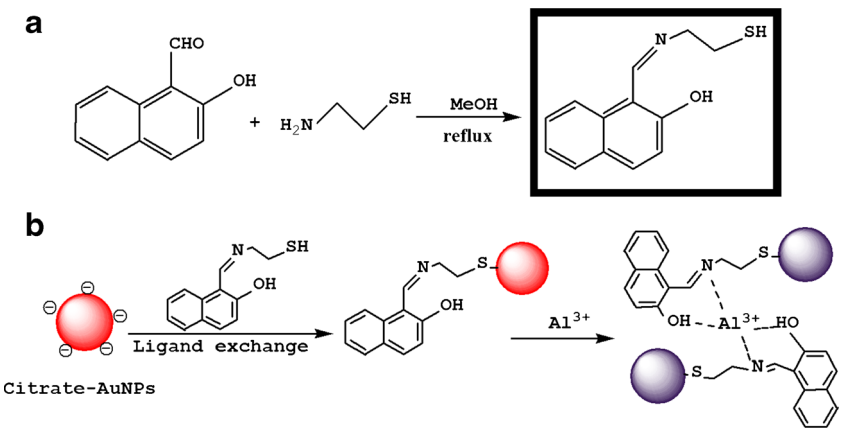

Scheme 1 **a** Synthesis of HNAET. **b** Illustration of ligand exchange of HNAET on the surface of AuNPs and signaling strategy for Al^{3+} based on the HNAET–AuNPs probe

hydrochloride was purchased from Sigma-Aldrich (http://www.sigmaaldrich.com/). Other chemicals used were of analytical grade or of the highest purity available. All the solutions were prepared using Milli-Q water (Millipore) as the solvent.

Synthesis of 1-(2-aminoethanethiol)-2-naphthol (HNAET)

According to previous reported literature [25], Briefly, to a solution of 2-hydroxy-1-naphthaldehyde (0.378 g, 2 mmol) in ethanol (25.0 mL), 5 mL 2-aminoethanethiol hydrochloride (0.227 g, 2.2 mmol) was added, and a amount of triethylamine was added in to adjust pH 7~8. The solution was stirred under reflux for 4 h and then allowed to stand at room temperature overnight as shown in Scheme 1a. The precipitate was filtered, washed thoroughly with ethanol and recrystallized with ethanol to give a luminous yellow powder, then dried under reduced pressure to afford compound HNAET in 90 % yield.

^{1}H NMR (400 MHz, DMSO) δ(ppm): 2.98 (t, 1H, SH), 3.14 (t, 2H, CH_2), 3.96 (t, 2H, CH_2), 6.76 (d, J = 12.0 Hz, 1H, ArH), 7.18 (t, 1H, ArH), 7.40 (t, 1H, ArH), 7.61 (d, J = 8.0 Hz, 1H, ArH), 7.72 (d, J = 8.0 Hz, 1H, ArH), 8.04 (d, J = 8.0 Hz, 1H, ArH), 9.11 (s, 1H, CH = N), 13.96 (s, 1H, OH) (Fig. S1). ESI-MS m/z: $[2M\text{-}H]^+$ calcd for $C_{13}H_{13}NOS$: 461.6; found, 461.1 (Fig. S2). Anal. calcd. for $C_{13}H_{13}NOS$: C 67.50, H 5.66, N 6.06, found C 67.52, H 4.75, N 6.01.

Synthesis of N-(2-hydroxynaphthylidene) -2-aminoethanethiol capped AuNPs (HNAET–AuNPs)

Citrate-capped AuNPs were prepared according to Frens' method [26]. All glassware were soaked in aqua regia and carefully cleaned before use. Briefly, 100 mL of 10 mM $HAuCl_4$ was taken into a round-bottomed flask and then boiled under vigorous stirring for 20 min. To this, 38.8 mM of trisodium citrate (10 mL) was added rapidly into the reaction flask and the mixture was stirred for another 15 min. The color of the solution changed from pale yellow to wine red, suggesting the formation of AuNPs. In order to remove excess sodium citrate, the citrate-reduced AuNPs were centrifuged for 15 min (1160×*g*) and then dissolved with Millipore-Q water. The concentration of the AuNPs was calculated according to Beer's law by using an extinction coefficient of *ca.* 10^8 M^{-1} cm^{-1} at 520 nm [27] and found to be 15 nM. To obtain HNAET-AuNPs, ethanol solution of HNAET (20 μL, 0.1 mM) was added into 10 mL AuNPs to let stand for ligand exchange reaction for 3 h to allow the modification of HNAET on the AuNPs surface at room temperature as shown in Scheme 1b. The resulting AuNPs solution was used for the colorimetric assay of Al^{3+} in real samples.

Signal response of HNAET-AuNPs probe to Al^{3+}

A stock solution of aluminum nitrate (1 mM) was prepared by dissolving aluminum nitrate in deionized water for the further use. For the detection of Al^{3+} by using the HNAET-AuNPs, 1.5 mL pH 6.0 HNAET-AuNPs (3 nM) aqueous solution was spiked with 0.5 mL Al^{3+} solutions to produce final concentrations in the range of 1.0–31 μM and the color of the solution changed from wine-red to purple then blue. The mixtures were then reacted at room temperature for 30 s and transferred for absorbance and photograph collection. The absorbance ratios of A_{620}/A_{520} versus Al^{3+} concentrations were used for calibration. Furthermore, we also evaluated the stability of AuNPs before and after functionalization. It was noticed that citrate modified AuNPs are stable for 2 months and well agreed with the literature [28]. At the same time, HNAET-AuNPs are stable for 3–4 weeks under nitrogen; after that there is a slight color change due to hydrogen bonding formation between HNAET-AuNPs. However, the rapid color change of HNAET-AuNPs solution (red to blue) was attributed to the HNAET-AuNPs aggregation induced by Al^{3+} ion (1.0–31 μM).

Results and discussion

Characterization of the HNAET–AuNPs

Gold nanoparticles were prepared through the citrate-mediated reduction of $HAuCl_4$. 1-(2-aminoethanethiol)-2-naphthol (HNAET) was added into the AuNPs solution as the capping agent. Figure 1A shows the UV–vis spectra of bare AuNPs and HNAET-AuNPs. It should be noted that the characteristic surface plasmon resonance (SPR) peak (520 nm) of AuNPs was slightly red shifted and the peak intensity was little decreased after functionalization of the HNAET molecules onto the surface of the AuNPs. We also investigated the batch-to-batch reproducibility when making HNAET-AuNPs, as shown in Fig. S3. The RSD is 2.32 % calculated by the absorbance at 520 nm, demonstrating good reproducibility of our approach for fabricating HNAET-AuNPs.

The characterization of decorated AuNPs was also studied in more details by using FTIR spectroscopy. FTIR spectrum of HNAET-AuNPs shows similar peaks characteristic to HNAET (Fig. 1B). It can be seen that for HNAET (Fig. 1B -a), -OH and -CH_2 stretches at 3000–3500 and 2913 cm^{-1}, respectively, and that the strongest absorption peak at 1629 cm^{-1} belongs to C = N stretching mode. These peaks can also be observed in the spectrum of HNAET-AuNPs (Fig. 1B -b). It can be noticed that the sulfhydryl group (-SH) stretching and bending modes were not observed at

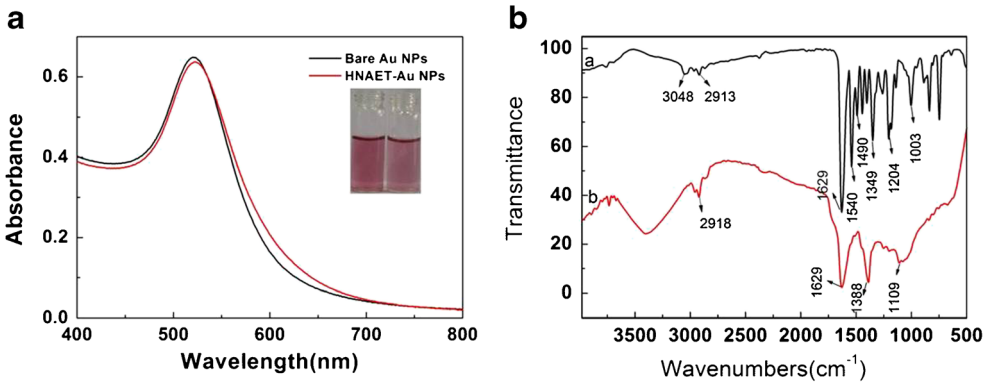

Fig. 1 **A** UV–vis spectra of bare AuNPs (*black line*) and HNAET-AuNPs (*red line*). Inset photograph shows the colors of bare AuNPs and HNAET-AuNPs. **B** FTIR spectra of (*a*) HNAET and (*b*) HNAET-AuNPs

2500–2600 cm^{-1} in the spectrum of HNAET, presumably due to the presence of the strongest absorption peak of C = N stretching. Besides, zeta potential of the AuNPs became less negative from −33.15 to −24.85 mV after functionalization, also indicating that some of citrates on the surface of the AuNPs were replaced by HNAET via ligand exchange because HNAET is nearly neutral. These results revealed that the HNAET molecules were successfully attached onto the surface of the AuNPs via Au–S bond. In addition, in Fig. 2B -a, the HNAET-AuNPs are well dispersed and from their size distribution (Fig. S4) according to the TEM image, the mean size of AuNPs is 12.4 ± 0.03 nm (100 particles counted).

The analyses of the ligand loading on surfaces of the AuNPs was measured by comparing the intensities at ca. 485 nm of supernatant solution of HNAET-AuNPs and pure HNAET solution before functionalization (Fig. S5). It is found that approximately 53 % of HNAET was bound onto the AuNPs, from which we can calculate the amount of ligands to be about 35 HNAET molecules per AuNP. We also investigated the long-term stability of HNAET-AuNPs under air and under nitrogen day to day, as shown in Fig. S6, ESM. It can be seen that HNAET-AuNPs showed higher stability under nitrogen than that under air since the later aggregated slightly after several days, which can be judged from the absorbance at 620 nm. Nevertheless, in view of fast response time to Al^{3+} (ca. 10 s), as demonstrated below, the relatively high stability of the AuNPs under air for about several days can absolutely fulfill the requirements in practical applications.

Detection mechanism for Al^{3+}

As show in Fig. 2A, for the initially well-dispersed HNAET-AuNPs, upon the addition of Al^{3+} (20 μM), the absorbance at 520 nm decreased greatly and a new absorption band at 620 nm appeared obviously. Accordingly, the color immediately changed from red to blue (inset in Fig. 2A). These changes were considered to be attributed to the aggregation of HNAET–AuNPs, which was also observed by TEM images (Fig. 2B-b). Furthermore, a gradual aggregation process of HNAET-AuNPs was also monitored by changes in the hydrodynamic diameter from particles to aggregates measured via DLS upon the addition of Al^{3+} at different concentrations (Fig. S7), in which the mean sizes of HNAET-AuNPs became larger gradually with the increase of Al^{3+} concentration.

Based on the above phenomenon, we suppose a possible mechanism to elucidate it. It is known that HNAET is a thiol-containing derivative of naphthol. After its functionalization onto AuNPs through Au-S bond, -OH and N atoms in C = N are effectively available to form a stable complex with Al^{3+},

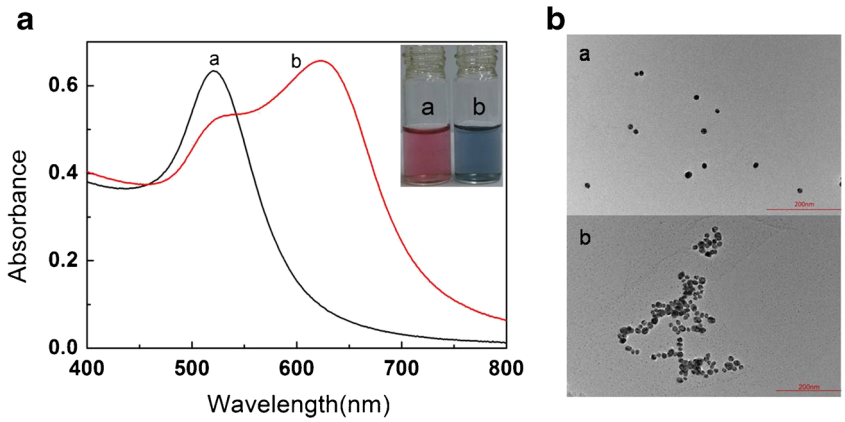

Fig. 2 (**A**) UV–vis absorption spectra and photographs (*inset*) and (**B**) TEM images of HNAET-AuNPs in the (*a*) absence and (*b*) presence of Al^{3+} (20 μM). The scale bar is 200 nm

which eventually induced the aggregation of HNAET-AuNPs. Thus, a fast and efficient interparticle crosslinking of the HNAET–AuNPs occurred in the presence of Al^{3+}. Scheme 1b summarizes the procedure for the working mechanism of the HNAET–AuNPs probe for Al^{3+}.

Optimization of reaction conditions

It is significant to choose optimal reaction conditions that determine enough aggregation of AuNPs, so the following parameters were optimized: (a) HNAET concentration; (b) sample pH value; (c) reaction time. Respective data and Figures are given in Fig. S8 and S9 in the Electronic Supporting Material. The following experimental conditions were found to give best results: the HNAET concentration at 2×10^{-7} M was chosen as the optimal ligand concentration, the optimal pH range for detecting by HNAET-AuNPs is 4–6, and reaction time was set at 10 s.

Selectivity of HNAET-AuNPs toward Al^{3+}

To investigate the analytical application of the HNAET-AuNPs toward various metal ions in aqueous solution, the UV–vis spectra of the synthesized HNAET-AuNPs were measured in the presence of metal ions such as Ag^{+}, Cd^{2+}, Co^{2+}, Al^{3+}, Cr^{3+}, Cu^{2+}, Fe^{3+}, Hg^{2+}, Mg^{2+}, Mn^{2+}, Ni^{2+}, Pb^{2+}, Ba^{2+}, and Zn^{2+}. Figure 3 shows the effect of the metal ions on the appearance of HNAET-AuNPs in solution. Al^{3+} was the only ion that caused a remarkable peak

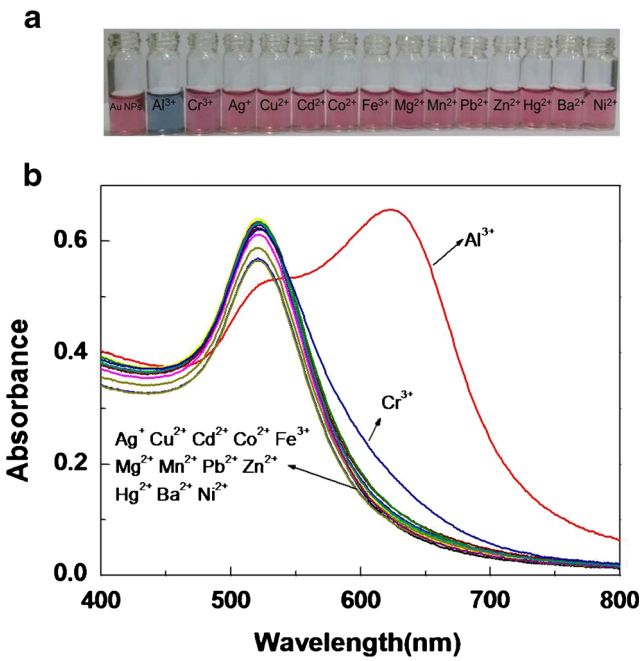

Fig. 3 **a** Photograph of HNAET–AuNPs in the presence of various metal ions (20 μM). **b** UV–vis absorption spectra of HNAET–AuNPs in the presence of different metal ions (20 μM)

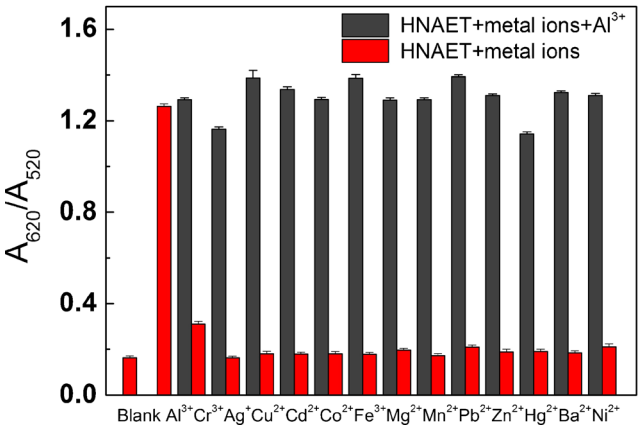

Fig. 4 Absorbance ratio (A_{620}/A_{520}) of HNAET–AuNPs in the presence of different metal ions. *Red bars* represent the addition of single metal ion (20 μM); gray bars represent a mixture of Al^{3+}(20 μM) with 20 μM Cr^{3+}, Hg^{2+} and 200 μM Ag^{+}, Cd^{2+}, Co^{2+}, Cu^{2+}, Fe^{3+}, Mg^{2+}, Mn^{2+}, Ni^{2+}, Pb^{2+}, Ba^{2+}, Zn^{2+}

shift of AuNPs from 520 to 620 nm. This red shift was directly observed as a color change from red to blue. The other metal ions did not influence the absorption spectra, indicating that no aggregation occurred. We reasoned that, as demonstrated above, strong and specific binding of Al^{3+} between the naphthol on HNAET-AuNPs induced the aggregation of the HNAET-AuNPs in which the naphthol functions as a metal ion chelator (Scheme 1b).

In order to study the influence of other metal ions on Al^{3+} binding to HNAET-AuNPs, competitive experiments were also carried out with Al^{3+} (20 μM) in the presence of other metal ions, namely Ag^{+}, Cd^{2+}, Co^{2+}, Al^{3+}, Cr^{3+}, Cu^{2+}, Fe^{3+}, Hg^{2+}, Mg^{2+}, Mn^{2+}, Ni^{2+}, Pb^{2+}, Ba^{2+}, and Zn^{2+} (Fig. 4). The plasmonic absorption shift caused by the mixture of Al^{3+} and another metal ion was similar to that caused solely by Al^{3+}. This result clearly indicates that our method was free from

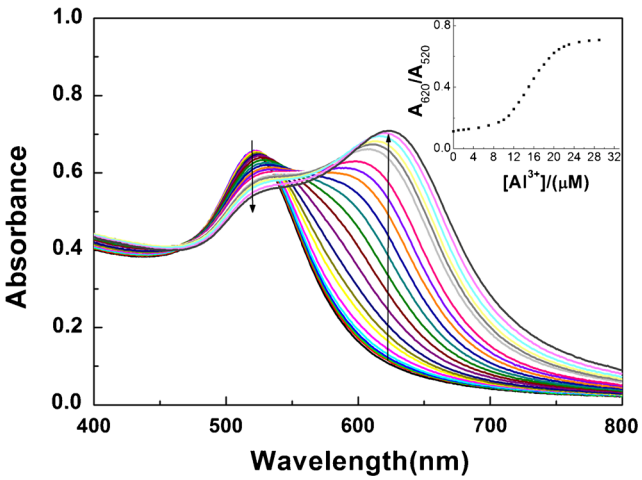

Fig. 5 UV–vis absorption change of HNAET–AuNPs in the presence of different concentrations of Al^{3+}. *Inset*: Plot of the absorbance ratios A_{620}/A_{520} against Al^{3+} concentration in the range of 0–24 μM

Table 1 Comparison of HNAET-AuNPs for the detection of Al^{3+} with the reported methods

Nanoparticles	Capping agent	Size(nm)	LOD(μM)	Detection method	Ref.
AuNPs	Citrate	17	1.0	UV–vis	[30]
AuNPs	5-mercaptomethyltetrazole	12	0.53	UV–vis	[31]
AgNPs	GSH	10	1.2	UV–vis	[32]
AuNCs	Tyrosine	1.96 ± 0.63	0.30	Fluorescence	[33]
AgAuNCs	Mercaptosuccinic acid	1.5	0.80	Fluorescence	[34]
CNDs	Quercetin	2.51	0.56	Fluorescence	[35]
AuNPs	HNAET	12	0.28	UV–vis	This study

interference from other metal ions, which should be noted for practical application to Al^{3+} assays in real samples.

Quantification of Al^{3+} by using HNAET-AuNPs as the colorimetric probe

The potential of the HNAET-Au NPs based UV–vis spectrometric method was demonstrated for the quantification of Al^{3+} in aqueous samples as a model analytical problem. At the optimized conditions, various concentrations of Al^{3+} were added into an HNAET-AuNPs solution and their UV-visible spectra were measured. Figure 5 shows that the color of the AuNPs in solution gradually changes from red via purple to blue on increasing the concentration of Al^{3+} which can be observed with bare eyes. Accordingly, the SPR peak of AuNPs at 520 nm decreased gradually, along with an increase of the SPR peak at 620 nm. Furthermore, a calibration curve was constructed between the absorbance ratio (A_{620}/A_{520}) and Al^{3+} concentration ranging from 9 to 23 μM ($y = 0.0743x - 0.452$, $R^2 = 0.990$) (Fig. S10), which can be used for the quantification of Al^{3+}. The detection limit (LOD) is 0.287 μM, which is much lower than the level (7.4 μM) of drinking water defined by the World Health Organization [29].

In addition, we also compared the sensitivity of the present method with the reported nanoparticle-based UV–vis and fluorescence methods for detection of Al^{3+} (Table 1). It indicates that the present method showed higher sensitivity than the nanoparticle-based UV–vis [30–32] and fluorescence [33–35] methods. Therefore, the present analytical system exploits the advantages of HNAET-AuNPs for the detection of Al^{3+} by using UV–vis spectrometry.

Application to the analysis of Al^{3+} in real samples

The present HNAET-gold nanoparticle-based colorimetric assay has been applied to detect Al^{3+} in aluminium pan water and urine samples. For this, aluminium pan water samples were obtained from distilled water boiled in aluminium pan. Human urine samples were collected randomly from healthy people and diluted 100-fold with ultrapure water. The above real samples spiked with certain amounts of Al^{3+} were determined according to the standard curve, and the analytical results are shown in Table 2. The recovery values ranged from 90 to 97 %, with the relative standard deviation (RSD) lower than 2.5 %. It suggests that the present method may be used in the detection of Al^{3+} in water quality monitoring and in urine sample testing.

Conclusions

In summary, a simple, cost-effective colorimetric assay for Al^{3+} based on the HNAET modified AuNPs is developed via ligand exchange. It is demonstrated that high affinity of Al^{3+} toward the N atom and the –OH of the Schiff base induces the aggregation of HNAET–AuNPs accompanied by distinct solution color change. Absorbance varies linearly with the Al^{3+} concentration in the range from 9 to 23 μM, and the detection limit is 0.29 μM. Because this method can address intrinsic limitations of small molecule-based optical sensors, such as complex synthetic procedures, low-sensitivity and poor water compatibility, it shows great potential in selective quantification of Al^{3+} in routine laboratory practice or rapid on-site assay. Additionally, further study is going on to avoid non-aqueous phase organic synthesis leading to a more environmentally-friendly colorimetric assay.

Table 2 HNAET-AuNPs for the analysis of Al^{3+} in real samples

Sample	Added (μM)	Found (μM)	Recovery (%)	RSD (%) ($n = 3$)
Aluminium pan water	10	9.3	93	1.18
	15	14.2	95	1.40
	20	18.0	90	2.50
Urine samples	10	9.5	95	0.82
	15	14.6	97	1.20
	20	18.5	92	1.23

Acknowledgements We gratefully acknowledge the financial support by Natural Science Foundation of China (no. 21365014, 21505067), Jiangxi Province Natural Science Foundation (JXNSF no. 20132BAB203011), and Doctoral Start-up Funding of Nanchang University.

Compliance with ethical standards

Conflict of interest The authors declare that they have no competing interests

References

1. Kepp KP (2012) Bioinorganic chemistry of Alzheimer's disease. Chem Rev 112:5193–5239
2. Mendez-Aèlvarez E, Soto-Otero R, Hermida-Ameijeiras A, Lopez-Real AM, Labandeira-Garc JL (2001) Effects of aluminum and zinc on the oxidative stress caused by 6-hydroxydopamine autoxidation: relevance for the pathogenesis of Parkinson's disease. Biochim Biophys Acta 1586:155–168
3. Wills MR, Savory J (1983) Aluminium poisoning: dialysis encephalopathy, osteomalacia, and anaemia. Lancet 2:29–34
4. Krejpcio Z, Wójciak RW (2002) The influence of Al^{3+} ions on pepsin and trypsin activity in vitro. Pol J Environ Stud 11:251–254
5. Frankowski M, Zioła-Frankowska A, Siepak J (2010) New method for speciation analysis of aluminium fluoride complexes by HPLC–FAAS hyphenated technique. Talanta 80:2120–2126
6. Chen B, Zeng Y, Hu B (2010) Study on speciation of aluminum in human serum using zwitterionic bile acid derivative dynamically coated C18 column HPLC separation with UV and on-line ICP-MS detection. Talanta 81:180–186
7. Wang H, Yu Z, Wang Z, Hao H, Chen Y, Wan P (2011) Preparation of a preplated bismuth film on Pt electrode and its application for determination of trace aluminum(III) by adsorptive stripping voltammetry. Electroanalysis 23:1095–1099
8. Arduini M, Felluga F, Mancin F, Rossi P, Tecilla P, Tonellato U, Valentinuzzi N (2003) Aluminium fluorescence detection with a FRET amplified chemosensor. Chem Commun 13:1606–1607
9. Maity D, Govindaraju T (2010) Pyrrolidine constrained bipyridyl-dansyl click fluoroionophore as selective Al^{3+} sensor. Chem Commun 46:4499–4501
10. Kim S, Noh JY, Kim KY, Kim JH, Kang HK, Nam SW, Kim SH, Park S, Kim C, Kim J (2012) Salicylimine-based fluorescent chemosensor for aluminum ions and application to bioimaging. Inorg Chem 51:3597–3602
11. Elghanian R, Storhoff JJ, Mucic RC, Letsinger RL, Mirkin CA (1997) Selective colorimetric detection of polynucleotides based on the distance-dependent optical properties of gold nanoparticles. Science 277:1078–1081
12. Liu J, Lu Y (2006) Preparation of aptamer-linked gold nanoparticle purple aggregates for colorimetric sensing of analytes. Nat Protoc 1: 246–252
13. Lee JS, Ulmann PA, Han MS, Mirkin CA (2008) A DNA–gold nanoparticle-based colorimetric competition assay for the detection of cysteine. Nano Lett 8:529–533
14. Saha K, Agasti SS, Kim C, Li X, Rotello VM (2012) Gold nanoparticles in chemical and biological sensing. Chem Rev 112:2739–2779
15. Sung YM, Wu SP (2014) Colorimetric detection of Cd(II) ions based on di-(1H-pyrrol-2-yl) methanethione functionalized gold nanoparticles. Sensors Actuators B 201:86–91
16. Chai F, Wang CG, Wang TT, Li L, Su ZM (2010) Colorimetric detection of Pb^{2+} using glutathione functionalized gold nanoparticles. ACS Appl Mater Interfaces 2:1466–1470
17. Chen GH, Chen WY, Yen YC, Wang CW, Chang HT, Chen CF (2014) Detection of mercury(II) ions using colorimetric gold nanoparticles on paper-based analytical devices. Anal Chem 86:6843–6849
18. Mehta VN, Kumar MA, Kailasa SK (2013) Colorimetric detection of copper in water samples using dopamine dithiocarbamate-functionalized Au nanoparticles. Ind Eng Chem Res 52:4414–4420
19. Lee YF, Nan FH, Chen MJ, Wu HY, Ho CW, Chen YY, Huang CC (2012) Detection and removal of mercury and lead ions by using gold nanoparticle-based gel membrane. Anal Methods 4:1709–1717
20. Liu R, Chen ZP, Wang SS, Qu CL, Chen LX, Wang Z (2013) Colorimetric sensing of copper(II) based on catalytic etching of gold nanoparticles. Talanta 112:37–42
21. Guo Y, Wang Z, Qu W, Shao H, Jiang X (2011) Colorimetric detection of mercury, lead and copper ions simultaneously using protein-functionalized gold nanoparticles. Biosens Bioelectron 26: 4064–4069
22. Li XK, Wang J, Sun LL, Wang ZX (2010) Gold nanoparticle-based colorimetric assay for selective detection of aluminium cation on living cellular surfaces. Chem Commun 46:988–990
23. Zhang M, Liu YQ, Ye BC (2012) Mononucleotide-modified metal nanoparticles: an efficient colorimetric probe for selective and sensitive detection of aluminum(III) on living cellular surface. Chem Eur J 18:2507–2513
24. Chang YJ, Hung PJ, Wan CF, Wu AT (2014) A highly selective fluorescence turn-on and reversible sensor for Al^{3+} ion. Inorg Chem Commun 39:122–125
25. Liu X, Lin Q, Wei TB, Zhang YM (2014) A highly selective colorimetric chemosensor for detection of nickel ions in aqueous solution. New J Chem 38:1418–1423
26. Frens G (1973) Controlled nucleation for the regulation of particle size in monodisperse gold suspensions. Nature 241:20–22
27. Huang CC, Chang HT (2007) Parameters for selective colorimetric sensing of mercury(II) in aqueous solutions using mercaptopropionic acid-modified gold nanoparticles. Chem Commun 75:1215–1217
28. Brewer SH, Glomm WR, Johnson MC, Knag MK, Franzen S (2005) Probing BSA binding to citrate-coated gold nanoparticles and surface. Langmuir 21:9303–9307
29. Guidelines for Drinking Water Quality (2004) World Health Organization, three edn. Geneva, 397, pp 301–311
30. Chen S, Fang YM, Xiao Q, Li J, Li SB, Chen HJ, Sun JJ, Yang HH (2012) Rapid visual detection of aluminium ion using citrate capped gold nanoparticles. Analyst 137:2021–2023
31. Xue DS, Wang HY, Zhang YB (2014) Specific and sensitive colorimetric detection of Al^{3+} using 5-mercaptomethyltetrazole capped gold nanoparticles in aqueous solution. Talanta 119:306–311
32. Yang NN, Gao YX, Zhang YJ, Shen ZY, Wu AG (2014) A new rapid colorimetric detection method of Al^{3+} with high sensitivity and excellent selectivity based on a new mechanism of aggregation of smaller etched silver nanoparticles. Talanta 122:272–277
33. Mu XY, Qi L, Qiao J, Ma HM (2014) One-pot synthesis of tyrosine-stabilized fluorescent gold nanoclusters and their application as turn-on sensors for Al^{3+} ions and turn-off sensors for Fe^{3+} ions. Anal Methods 6:6445–6451
34. Zhou TY, Lin LP, Rong MC, Jiang YQ, Chen X (2013) Silver–gold alloy nanoclusters as a fluorescence-enhanced probe for aluminum ion sensing. Anal Chem 85:9839–9844
35. Zou Y, Yan FY, Dai LF, Luo YM, Fu Y, Yang N, Wun JY, Chen L (2014) High photoluminescent carbon nanodots and quercetin-Al^{3+} construct a ratiometric fluorescent sensing system. Carbon 77: 1148–1156